Approved For Release STAT
2009/08/26 :
CIA-RDP88-00904R000100110

**Third United Nations
International Conference
on the Peaceful Uses
of Atomic Energy**

Confidential until official release during Conference

EXPERIMENTAL STUDIES ON FAST-NEUTRON REACTOR PHYSICS

A.I.Leipunskii, I.I.Bondarenko, O.D.Kazachkovskii, L.P.Abagyan, Yu.S.Aborin, N.O.Bazazyants, G.A.Batirbekov, V.V.Bondarenko, A.I.Voropaev, V.I.Golubev, E.F.Efimov, Yu.S.Zamyatkin, A.V.Zvonarev, V.P.Zinovyev, M.N.Zyzyn, V.V.Ivanov, N.V.Krasnoyarov, N.N.Krot, M.Ya. Kulakovskii; V.G.Liforov, V.F.Mamontov, B.K.Maslennikov, V.I.Matveev, V.N.Morozov, M.N.Nikolaev, M.Yu.Orlov, V.A.Parfyonov, V.V.Penenko, V.E.Ridkii, V.A.Semyonov, G.N.Smirenkin, A.P.Smirnov-Averin, V.P.Sokolov, M.F.Troyanov, O.P.Uznadze, F.I.Ukraintsev, L.N.Usachev, N.N.Shagalin.

The results of research work on physics of fast reactors are reported. This work was carried out in the Institute of Physics and Energetics of the State Committee on Uses of Atomic Energy of the USSR since the Second UN Conference on peaceful uses of atomic energy held in Geneva and was done as the continuation of investigations reported there [1].

MULTIGROUP CONSTANT SYSTEMS

Multigroup method is often used now for calculations in fast reactor physics. All the neutrons are divided into a finite number of energy-groups in this method.

In the early developments of this method the constant sets with a small number of groups were used to cover the neutron energy range of interest for fast reactors. [1], [2]. Such systems are very convenient in the case of reactors with highly concentrated cores and heavy, strongly absorbing reflectors, when neutron spectra have relatively well defined lower limit. However they hardly are of great use for calculations of large power reactors, especially ones with oxide or carbide fuel. The elastic moderation of neutrons plays considerable role in these reactors and lower limit of the spectrum becomes indefinite. It is very desirable in these conditions to have constant systems including all the neutron energies down to thermal ones. The 18- and 21-group systems meet these requirements rather well [3]. They have been widely used in our Institute during some time up to recently. Now we use 26-group system [4] which is set as principal in this report.

THE EXAMINATION OF LARGE REACTOR SYSTEMS AT THE "BFS"-STAND

The investigations on physics of large fast power-reactors with highly diluted fuel were carried out on the "BFS"-stand designed specially for this purpose (see Fig. 1).
The device will be described in detail in the "Atomnaya Energiya".

T h e   c h a r a c t e r i s t i c s   o f   s y s t e m s   e x a m i n e d. More than 15 reactor systems were examined at "BFS" since its setting into operation (June 1961). Four typical examples are considered in this report. The parameters of these systems are presented in Table 1. In the first three systems the fuel was diluted in active zone practically by a single element – nickel, iron or uranium. The experiments of this kind allow to find out the errors of constants of basic dilutors now in use for fast reactors construction and to estimate the accuracy of accounting of various physical effects (for example, resonance cross-section structure etc.). In the fourth case the system was a physical model of industrial power-reactor with ceramic fuel.

T h e   i n t e g r a l   p a r a m e t e r s. The most important reactor characteristics are integral parameters: critical mass, breeding ratio and others. Experimental and calculated values of these parameters are shown in Table 2. Experimental and calculated values of critical mass may be compared in 2 different ways: calculated critical mass be determined either by the variation of the composition with fixed size or vice versa. Calculations were made in 18-group P_1-approximation on the basis of 26-group cross-sections [4] by the method of approximate separation of variables. The corrections due to the difference between real geometry of system and that of ideal cylinder were calculated by application of perturbation theory and introduced into results. These corrections are small (no more than 0.2% in critical mass). The second method of critical mass determination (by variation of the core's diameter) results in somewhat greater values. The difference between these two methods is demonstrated by the data in Table III. Heterogeneous resonance effects only were taken into account in the evaluation of critical masses [6]. Nonresonant homogenity was not considered; this effect can contribute as much as 5% to critical mass of some systems. That is confirmed by experiment ("BS-8" critical mass has been decreased by 4.5% with U^{235}-heterogenity increasing at constant radius). Two-dimensional calculations were made in addition to approximate variables separation calculations. Critical mass of "BS-12"-system determined by 18-group two-dimensional computation practically coincides (within 1%) with the result of one-dimensional computation thus confirming a good efficiency of the conditional variable separation method. It must be noted that reasonable agreement between experimental and computed values was obtained taking into account the resonance effects for each system individual. The most striking example of this type is "BS-8"-system. The critical mass calculated without selfshielding consideration was 15% less than experimental value (with constant size of the .ore). Experimental ratios of the total number of events shown in Table 2 result from numerical two-dimensional integration of experimental data. Calculated ratios are, as a rule, in reasonable agreement with empirical values. The most essential deviations occur for the ratio of numbers of fission-events in U^{238} and U^{235} (f_8^{a3} / f_5^{a3}) in the core of "BFS-12". The main part of this difference is due to the heterogenity of experimental system which was not taken into account in calculations.

Neutron capture in U^{235} could not be measured at "BFS"-stand and it was consequently impossible to derive the breeding ratios for systems examined from the experimental data only.

368   — 2 —

The ratios $a = \sigma_c(U^{235})/\sigma_f(U^{235})$ obtained by multigroup calculations with constants [4] were used for the determination of breeding ratios on the basis of experimental values. Breeding ratios thus determined are in reasonable agreement with purely calculational values.

The number of events distribution. It was demonstrated above that the usage of approximate variables separation method with the proper constant system provides good accuracy in the calculations of integral characteristics for large reactor systems. The satisfactory results were obtained by application of this method to the evaluation of space-distribution of number of events in reactor. For example, such distributions for "BFS-12" system are shown in Fig.2. The results of 18-group two-dimensional calculations are given there also. The difference between one- and two-dimensional calculations becomes considerable in the last layers of the blanket only. The satisfactory agreement exists between experimental and theoretical results.

The characteristics of core-materials. The radial trend of cross-sections ratios of various reactions for "BFS-12" system is shown in Fig. 3. Even the ratio of U^{238} (n,f) and U^{235} (n,f) cross-sections which depend on energy in very different ways is constant in the core. It indicates that neutron spectrum is constant in the central part of the core and consequently space-distribution of neutrons can be described by one-group model. In one-group theory neutron space-distribution in the core is known to coincide with the distribution in the critical bare reactor and is completely determined by the single value — the material parameter x^2.

The notes separation of spatial and energetic variables in the central parts of the core occurs for all the systems examined.

In these regions energy spectrum and spatial distribution of neutrons are completely determined by the "nuclear" physical characteristics of the medium and it is very valuable because a possibility arises for the verification of constant sets for multiplying media. This possibility is affected neither by the accuracy of reflector's constants nor by the correctness of mathematical and geometrical approximations made (in so far as characteristics of the bare reactor may be calculated exactly).

Though no detailed measurements of neutron spectra in the cores of the described systems were made, observed ratios of average cross-sections of reactions with different energy dependence may be taken as integral characteristics of these spectra. These parameters are compared in Table 1 with the values resulting from averaging of cross-sections for the spectra in bare critical cores. The experimental and theoretical values of the material parameter x^2 are compared in the same Table. For the calculation of these values experimental distributions were approximated by eigenfunctions of the cylindrical model by using least-squares method.

Experimental and theoretical values are found to be in reasonable agreement. The discrepancy essentially larger than experimental uncertainty occurs in the single case — for the ratio of fission cross-sections of U^{238} and U^{235}. The heterogeneity of "BFS-12"-assembly mentioned above is responsible for this disagreement.

Distortions. The reactivity perturbations produced by various substances introduced into reactor's core were also measured on "BFS"-assemblies. Some of these results are presented

In Table 5. The size of samples were choosen small enough to avoid the distortion of neutron distribution and to make the first-order calculations of perturbation theory sufficiently accurate. The results shown demonstrate the reasonable agreements between theory and experiment. Spatial distribution of distortions were examined in addition to the distortion in the centre of the core. Experimental and theoretical distributions of reactivity introduced by various substances are shown for "BFS-12"-assembly in Fig. 4.

THE EXPERIMENTS ON NEUTRON DIFFUSION IN MEDIA

To find out the sources of possible errors in reactor calculations macroscopic experiments are of great help especially ones carried out with these sources   definitely removed at certain (at least partially – the experiments with simple geometry, in uniform media etc.).

Now we consider the results of experiments of this kind concerning neutron diffusion in moderating simply composed media with low multiplication. The major part of [1] these measurements was carried out at the "BR-1"-reactor and consisted in the examination of neutron space-energy distributions in the thick reactor blankets composed of various materials. The concentrated plutonium core of "BR-1"-reactor worked as the neutron-source with the spectrum very close to fission spectrum. Experimental technique is described elsewhere [1], [7], [8]. The results obtained at "BR-1" are complemented by detailed time-of-flight measurements on the reactor "IBR" [9]. The experimental arrangement is outlined in Fig.5. The neutrons escaped the prism under examination were detected by scintillator [10] disposed at the distance (1km) from reactor's core. The resolution was ~ 0.04 $\mu sec/m$ in this case.

The media containing uranium. U^{238} plays an important part in the fast breeders and the considerable part of experimental program carried out at "BR-1" was devoted to the examination of uranium-containing media.

In addition to metal uranium (the results on this subject were reported on the 2-nd Geneva Conference) [1] uranium's oxide and heterogeneous graphite-uranium assembly modelling uranium's carbide were examined.

It is interesting to compare some general nuclear-physical characteristics of these materials, for example, characteristics averaged over equilibrium and a., .ptotic neutron spectra in the various media [1]. The asymptotic and equilibrium neutron spectra in uranium carbide were examined in the blanket of "BR-1" composed of the cylindrical slugs (diameter 47 mm) of uranium metal (h = 2 cm) and of graphite (h = 1 cm) packed into close hexagonal lattice [11]. Uranium and graphite densities in this system were $2.74 \cdot 10^{22}$ and $2.42 \cdot 10^{22}$ nuclei/cm^3 respectively.

Heterogeneous effects in the examined assembly were not large ($\leqslant 15\%$) and were taken into account both in theory and experiment. Blanket's dimension in the direction examined was large (up to 80 cm). At the distances more than ~ 50 cm from the core the asymptotic equilibrium of neutron spectrum existed, appearing in the constancy of ratios of reactions cross-sections with essentially different energy dependence (see Fig.6). The integration of experimental distribution over the blanket total volume made the evaluation of equilibrium spectrum characteristics to be possible (after introducing small corrections $\leqslant 5\%$ due to the
368

– 4 –

leakage). In the case of uranium's oxide only the characteristics of asymptotic spectrum were measured in the exponential experiment with the prizm 139.4x104x112.2 cm. Its composition is shown in Table VI.

The copper blanket of "BR-1" served as neutron source. The characteristics of asymptotic and equilibrium spectra obtained in these experiments are presented in the Tables VII and VIII. The utilization coefficient D, presented in Table VII describes the multiplication of fission neutrons in the medium because of fission of U^{238} [1].

This parameter decreases in the carbide and oxide of uranium (D = 0.118±0.009) due to the removal of neutron under the fission barrier of U^{238} after moderation on the nuclei of carbon, oxigen and other impurities. Another important parameter is the asymptotic diffusion-length. For convenience the inverse value divided by the density of uranium (nuclei per cm^3) is shown in Table VII. The increase of this parameter in carbide and oxide relative to the metallic uranium means that by using these compounds the total quantity of uranium in the blanket providing the given level of neutron leakage may be reduced. This fact results in the partial compensation of the additional removal caused by the presence of the carbon and the oxygen. Then the relative contribution of U^{238} fission in the total neutron balance remains constant in the asymptotic regions of all examined media containing uranium (which is confirmed by the constancy of the ratios $\sigma_f(U^{238})/\sigma_f(U^{235})$. Experimental and calculated characteristics of asymptotic and equilibrium neutron spectra in the uranium-containing media including the ratios of average cross-sections of reactions with different energy dependence are in reasonable agreement. In the case of carbide and oxide this agreement was achieved only due to accounting of resonance selfshielding of cross-sections in the constant system used. This effect is the largest for uranium oxide, where capture cross-section increases by 10±3% due to the Doppler-broadening of resonances when the sample irradiated is heated from $300^{\circ}K$ to $900^{\circ}K$. The calculated figure is 9%.

The spatial neutron distributions in the uranium-containing media are described satisfactorily too (see Figs 6 and 7).

T h o r i u m. The possibilities of the utilization of thorium for power-production are usually considered in connection with the feasibility of breeding cycle for the thermal reactors. However bearing in mind the possibility of the utilization of the total resources of the nuclear raw materials and the production of U^{233} it is desirable to consider the utilization of thorium in the fast breeders in particular as a material for the construction of the outer breeding zone. In this connection it is interesting to measure the nuclear characteristics of thorium and to compare them with those of uranium. To attain this object the thorium control rods were mounted at "BR-1" (see Fig. 8) and a thick thorium blanket was assembled (110 cm high, 120 cm thick) of cylindrical thorium blocks 35 mm-diameter. To decrease the neutron leakage through the chinks between blocks the successive layers were shifted one relative to another by the half of the lattice pitch. The average density of thorium was $2.61 \cdot 10^{22}$ nuclei/cm^3.

The measurements of total number of events in reactor allow to determine the breeding ratio of such a system. This value (2.05±0.09) was in agreement with the calculated figure 1.97 (the theoretical value of $\alpha = \dfrac{\sigma_c(Pu^{239})}{\sigma_f(Pu^{239})}$ was used in both cases which was equal to 0.06).

368

– 5 –

The reduction of breeding ratio in thorium reactor relative to the identical system with uranium blanket (2.5±0.1) [1] is due to the decreasing of contribution of fission in the raw material from 0.5 to 0.070±0.003. The contribution of $Th^{232}(n, 2n)$ reaction to the breeding ratio is estimated as 0.011±0.001.

The parameters of equilibrium neutron spectrum in thorium are given in Table VIII. The experimental and theoretical values of the utilization coefficients are presented in the same Table. It is difficult to explain the observed difference between these two values by the experimental uncertainty only. In so far as thorium's fission cross-section (68mb) used in calculations is in good agreement with the results of direct measurements (60mb) the error in the values of utilization coefficients included in the constant system used is the probable source of the discrepancy. One needs to take $D = 2.3±0.2$ barn to avoid this disagreement.

There is no asymptotic equilibrium spectrum in thorium but shape of the spectrum of neutrons absorbed in thorium varies slowly (see Fig. 9) and consequently the spatial distribution of captures at the distances from the core exceeding 20~40 cm may be described satisfactorily by one-group approximation. The inverse diffusion length for this group divided by thorium density (nuclei/cm^3) equals 2.6±0.1 barn exceeding the corresponding value $\mathscr{x}/N_8$ for asymptotic spectrum in uranium (see Table VII). The space-energy neutron distributions near the source are complicated and must be treated by multigroup methods. The comparison of multigroup results with experimental data shows that the constant system [4] provides the satisfactory accuracy of calculations (see Fig. 9).

The moderating media-nickel, iron, copper. The examination of neutron diffusion in moderators is of interest for the shielding problems and for the reactor physics in general. Actually the concentration of moderative dilutors in the cores of large power fast breeders is found to be high; reactor's blankets contain the considerable quantities of coolers and construction materials and in special case (as for example in BR-5 reactor) blanket consists entirely of nonmultiplying elements [13].

The problem of taking into account the cross-section resonance structure is one of the main problems when the neutron diffusion in moderating materials is considered. Light and middle nuclei (A ≈ 50) show cross-section structure up to energies of some Mev [14]. It should be noted that in contrast to the heavy nuclides in the case of light and middle nuclei not only neutron absorption, but also moderation and transport depend on the cross-section resonance structure.

When the cross-section resonance structure in Kev region is to be considered the situation is complicated by the presence of resonance-potential interference. At higher energies the resonance-resonance interference also is to be taken into account [6]. These complicative circumstances reduce considerably the reliability of the group constants in macroscopic experiments. Here are considered the results of some experiments of this kind.

Fig.10 shows the distribution of different reactions in the nickel blanket of BR-1 reactor as well as the calculation of these density distributions carried out with and without the consideration of the cross-section selfshielding. The discrepancy between experiment and calculation shows that the used constants overestimate selshielding effects. The same

— 6 —

conclusion follows from the comparison of the calculated spectra of neutrons emerging from nickel prism with time-of-flight results (Fig. 11). One can see that the most striking discrepancy between the experiment and calculation takes place in the vicinity of the cross-section interference minima at 10 Kev and 150 Kev. It is not surprising since the cross-section structure for nickel is poorly known and available constants include rather large uncertainties. To improve the agreement between calculation and experiment it is necessary to vary cross-section selfshielding coefficients for neutron groups corresponding to these interference minima by 20-30% [21] (Figs 10-12).

The total cross-section of iron which consists mainly of the only Fe^{56} isotope demonstrates the interference of resonance scattering and potential scattering especially distinctly. Most prominent dip locates at 29 Kev where neutron free path has a value 70cm. Under higher energies the iron cross-section also shows interference minima. That is why the reliability of the description of the neutron space-energy distribution in Fe depends strongly on the accuracy of taking into account the neutron leakage This leakage is always considerable for the large iron blocks. So the accuracy of mathematical approximations used in calculations as well as group constants accuracy are of major importance. It seemed to be interesting to investigate the neutron diffusion in iron.

The "BR-1" reactor with iron blanket was used for such an investigation. The reactor construction was the same as described in [1] with the only exception that blanket thickness in the direction used for measurements was chosen to be 91 cm. The cross dimensions were 70cm x 74cm.

The results of measurement of different reactions in this blanket are presented in Fig. 13. The discrepancy of one-dimensional calculation in P_3-approximation with the experimental results in the core is because of the difference in calculated (8,38cm) and measured (6,96cm) values of critical radius. This discrepancy may be explained by two reasons. First, in P_3-approximation the neutron leakage from the core is considerably overestimated (the core radius was only 1.5 neutron free path). Second, the cross-section selfshielding effects described in [4] were considered only in average. In the blanket layers close to the core the neutron spectrum structure varies strongly with the distance. Selfshielding coefficients vary correspondingly. But this variation cannot be accounted in terms of usual multigroup calculation. So the cross-sections for the nearest iron layers are consequently underestimated because of the resonance selfshielding effects. As a result the blanket albedo characteristics are diminished and the critical mass becomes overestimated.

It is easy to see that the second reason dominates.

Really, the calculated critical radius for the reactor with the German silver control rods and nickel blanket exceeds experimental value only by 6%. Two-dimensional calculation is carried out for the real-sized core; the criticality of the system had been reached by the variation of ν-value for Pu^{239} in the core. In this way one was capable to compensate considerably the effect of aforementioned reasons on the neutron space-energy distributions.

This example demonstrates that usual multigroup calculation of the system possessing sufficient leakage and strong resonance selfshielding of the cross-sections may result in

appreciable uncertainties. To avoid these uncertainties one has to consider selfshielding effects more correctly than it is usually characteristic for multigroup calculations. The subgroup method [6], for example, may serve for this purpose.

The averaging of iron constants over the infinite medium spectra in regions far from the core (recommended by [4]) is reliable and hence in these cases the discrepancies in space-energy distributions result from the certainties in iron cross-section data used and uncertainty introduced by the idealization of the system geometry. As it could be shown from Fig. 13 experimental values are in the best agreement with spherical geometry calculation. This agreement however is illusive because the leakage through the side surface of the prism could not be taken into account in this case. When this leakage is taken into account by two-dimensional calculation in P_1-approximation with the same constants the agreement fails. The low energy neutron flux is especially sensitive to the neutron leakage. For example, neutron flux decreases by a factor of two after averaging over gold capture cross-section. Taking into account the great leakage in P_1-approximation is known to be unreliable and results in the overestimate of the leakage which corresponds approximately to the factor of 1.5 in our case.

More correct leakage consideration would improve the agreement between experiment and theory. Nevertheless it is clear that even in this case the discrepancy could not be avoided. The nature of these discrepancies gives the evidence that resonance selfshielding effects were overestimated when iron cross-section (especially transport cross-section) had been calculated. It obviously refers mainly to the neutron group corresponding to interference minimum at 27 Kev. At this energy the total cross-section value includes maximum uncertainty. This conclusion has been qualitatively confirmed when experimental energy spectrum of neutrons leaving the iron prism has been compared with the calculated spectrum (Fig. 14). The calculation for these systems was carried out in plane geometry by using the S_n-approximation. The leakage through the side surface was taken into account by adding some fictious absorption cross-section. However, it should be pointed out that the most rigid requirements to the reliability of constants to be used arise when the medium consisting of the only element with resonance cross-section structure is considered. In the most important practical case for the mixture of same elements these requirements are considerably reduced. For example, in the case of stainless steel 1 x 18H9T the description of the neutron spectrum by our constant set was satisfactory (Fig. 15).

The results of the examination of the neutron space-energy distribution in the copper blanket of BR-1 reactor had already been reported at the Second Geneva Conference in 1958, so only the comparison of some of these results with multigroup calculation data is given in this report (Fig.16). It should be noted that in the case of copper the description of experimental distributions also requires the correct consideration of the resonance selfshielding effects.

NEUTRON SPACE-ENERGY DISTRIBUTIONS AT THE TWO MEDIUM BOUNDARY

As follows from the above discussion the application of group constants taking into account resonance selfshielding effects and supposing the collision density to be constant provides

368

— 8 —

reasonable accuracy of neutron space-energy distribution calculation in the continuous media but could fail when a region near boundary is considered. Since the determination of neutron flux distributions is sometimes of considerable interest, a series of experiments on studying the boundary resonance effects is now under development at the "BR-1" reactor. The first of them were devoted to the investigation of the increment of neutron-flux density at fast reactor blankets when the latter is surrounded by the additional reflectors from different materials [15].

Up to now the measurement of neutron space-energy distributions has been carried out at the boundaries of uranium blanket [16], uranium-carbon blanket [17] and thorium blanket which had been surrounded by an additional iron, stainless steel, nickel, copper, berillium, carbon and water reflectors. Figs 19-21 demonstrate the change of resonance cross-section selfshielding near the boundary. The measured capture density in this regions prominently exceeds the calculated one. At the same time the measured flux of resonance neutron ($E_n = 4$ 9ev) which penetrates into the blanket from the additional reflector drops more steeply than the calculations predict. These results are of practic importance. In fast breeders it is useful for the suppression of neutron leakage from the breeding zone to surround the latter by additional reflector. So the question arises: what material would be the best for this purpose? The measure B of the efficiency of additional reflector is the increase of neutron capture events within the blanket due to the additional reflector divided by the difference between the number of neutron capture events within the blanket in two cases: the infinitely thick blanket and the chosen blanket.

The parameter for the investigated blanket and reflector materials is presented in Table IX. The quantities Δ of the fuel economy which could be reached because of additional reflector application (with breeding ratio being constant) are also given. Large uncertainties of the quantities presented in Table IX are due to the fact that the measured effect is the small difference between two large quantities.

It is easy to see the greatest value of considered characteristics must be incorporated to berillium. However the spectrum of neutrons returning from the additional reflector depends essentially on the reflector material and if so above mentioned values must not be decisive for the choice of additional reflector. It is very important to know the rate of burning and the shape of neutron spectrum in the produced fuel.

MEASUREMENTS OF NEUTRON RADIATIVE CAPTURE BY URANIUM AND THORIUM ISOTOPES FOR THE REACTOR SPECTRA

For the determination of some reactor characteristics (such as breeding ratio, critical mass etc.) it is necessary to know the distribution of neutron radiative captures in fissible materials throughout the reactor. The calculation of this quantity is unreliable at present because of uncertainty in values of radiative capture cross-sections for fissible isotopes. Its direct measurement at little power critical assembly also seems to be impossible. So with the mono-energetic neutrons used the only way of measurement of this cross-section is the detection of

368

capture γ-rays. This technique is very complicated by a strong background and by the weakness of the effect which is to be measured. The results of such experiments still have large uncertainties. Also a number of complications [6]preventsan application of the capture cross-section data, received in the resonance region by time-of-flight technique.

In this situation the measurements of capture cross-sections of fissible isotopes for wide neutron spectra are of considerable interest. Such a possibility arises when a powerful reactor is used. Here it becomes possible to store a sufficient number of nuclei produced by neutron capture in the sample. The concentration of these nuclei then can be determined by the mass spectrometric methods. The results of such measurements carried out at BR-5 [13] reactor are given below. The peculiarity of spectrum of this reactor is its strong variation from the concentrated plutonium core to the nickel blanket'[18]. This circumstance allowed to fulfil the measurements of capture cross-section and relation $a = \sigma_c/\sigma_f$ for wide range of neutron spectra including nearly all energies of practical importance. The following experimental procedure was applied. Samples of uranium protoxide-oxide and plutonium oxide 6-8mg weight were packed in brass covers (envelopes) and then placed inside the airtight (hermetical) envelope of stainless steel. This experimental arrangement was put in the reactor core instead of one of nuclear fuel slug at the distance 4, 7 cm from vertical axis of the reactor.

Samples placed at the central plane of the reactor were radiated by a total number of $1.14 \cdot 10^{22}$ neutrons per square centimetre during nearly five months of reactor operation [18] . After some delay necessary for reducing γ-back-ground the samples were radiochemically treated to extract the probes for mass-spectroscopic and radiometric analysing.

The mass-spectrometer results serve to determine quantities of nuclei produced by the neutron radiative capture by U^{233}, U^{235} and Pu^{239} nuclei. The concentration of Pu^{240} in isotopically pure Pu^{239} (the concentration of Pu^{240} before irradiation $5 \cdot 10^{-3}\%$) was also determined by measuring the spontaneous fissions of irradiated samples [19]. There is a reasonable agreement $(2 - 5\%)$ between the results of these two independent measurements.

The distribution of fission events was measured by ionization chamber and by the radiochemical methods detecting the radioactivity of extracted fission fragments.

With the total neutron flux and concentrations of accumulated U^{234}, U^{236} and Pu^{240} known it is possible to determine the capture cross-sections U^{233}, U^{235} and Pu^{239} respectively and their ratios to the fission cross-sections.

Tables X — XII present the measured and the calculated values of σ_c, σ_f and $a = \sigma_c/\sigma_f$ for the uranium and plutonium isotopes investigated and some specific neutron spectra of BR-5 reactor. The forms of these spectra are shown in Fig. [20]. The neutron spectrum calculation was carried out for idealized homogeneous spherical reactor with using multigroup constants recommended in [4].

The impossibility of exact taking into account the complicated geometry of real reactor did not allow to obtain a good agreement between experiment and calculation for the space distributions. Nevertheless calculated cross-section ratios appeared to be in reasonable agreement with the experimental results. This fact (as well as the verification of accuracy of spectrum calculations in the macroscopic experiments discussed above) permits to suppose

368

that the calculated spectra were close to real ones. So a rather good agreement of experimental and calculated data on capture cross-sections could be interpreted as a confirmation of correct values of radiative capture and fission cross-section used in calculation.

The greatest discrepancy much exceeding experimental uncertainty takes place for capture cross-section of Pu^{240}. Obviously, group cross-sections for this isotope chosen corresponding to the recommendations of [20] and semitheoretical considerations of [4] are overestimated appreciably.

REFERENCES

1. *A.I.Leipunsky et al.* Second Geneva Conference report No.2038. Geneva, 1958.
2. *I.V.Gordeev, D.A.Cardashev, A.V.Malishev.* Nuclear physics constants. Atomizdat. Moskow, 1960.
3. *G.I.Marchuk.* The methods of nuclear reactor calculations. Gosatomizdat, Moscow, 1961.
4. *L.P.Abagyan* et al. The group constants for the reactor calculations. M. Gozatomizdat, Moscow, 1964.
5. *L.P.Abagyan* et al. "Group Constants for Designing Nuclear Reactors", Consultants Bureau Enterprises, inc., N.V.(to be published).
6. *L.P.Abagyan* et. al. Report presented at this conference.
7. *M.N.Nicolaev* et al. Report N86 "Physics of fast and intermediate reactors", IAEA. Vienna, (1962).
8. *V.I.Golubev et al.* "Neutron resonance indicators in the investigations of neutron spectra in fast reactors". "Atomnaya Energiya", II, 522, 1961.
9. *G.E.Blohin* et al. "Report N 81. Physics of fast and intermediate reactors, page 309, IAEA, Vienna, (1962).
10. *I.Vizi* et al. Liquid scintillators for neutron detection Annals of conference on nuclear electronics, Belgrad, 1961.
11. *V.I.Golubev* et al. The neutron diffusion in uranium carbide. "Atomnaya Energiya", (to be published).
12. *I.I.Bondarenko, V.P.Covaliov.* "Pile neutron research in physics", page 159, IAEA, Vienna, (1962).
13. *A.I.Leipunsky* et al. Second Geneva Conference, report No.2129, Geneva, 1958.
14. *M.N.Nicolaev* et al. Report N 85. "Physics of fast and intermediate reactors", page 65, IAEA, Vienna, (1962).
15. *M.N.Nicolaev* et al. Report N 87.
16. *V.I.Golubev* et al. "Atomnaya Energiya", 15, 258 (1963).
17. *V.I.Golubev* et al. "Atomnaya Energiya", 15, 327 (1963).
18. *A.I.Leipunsky* et al. "Physics of fast and intermediate reactors", page 315, IAEA, Vienna, 1963.
19. *V.N.Ivanov, N.N.Crot* and *G.N.Smirenkin.* "Atomnaya Energiya" (to be published).
20. *Uiftah, Okrent* and *Moldauer*, Fast Reactors Cross-sections, New York, Pergamon Press, 1960.

Parameters of experimental assemblies

Table 1

Parameters			BFS-1A	BFS-6A	BFS-8	BFS-12
Height of the core, [cm]			22.6	53.4	63.84	120.85
Eq. diameter of the core, [cm]			29.3	57.9	72.83	100.6
Volume, [liter]			15.3	140.7	266.0	960.7
Critical mass, [kg U^{235}]			76.5	239.5	343.3	709.4
Side blanket thickness, [cm]			38.0	29.0	35.5	30.9
Upper blanket thickness, [cm]			90.0	58.5	60.0	40.0
				28.5		
Composition (volume %)	Core	U^{235} (18.8g/cm^3)	26.6	9.15	6.94	3.97
		U^{238} (18.6g/cm^3)	3.12	62.86	0.81	17.35
		Iron (7.8g/cm^3)	0	0	65.87	17.40
		Stain. (7.9g/cm^3) steel	11.06	12.08	12.43	6.84
		Nickel (8,9g/cm^3)	39.16	0	0	0
		Aluminium (2.7g/cm^3)	4.74	1.58	1.24	18.32
		Graphite (1.6g/cm^3)	0	0	0	17.67
		Air	15.32	14.33	12.71	18.45
	Side blanket	U^{238} (18.8g/cm^3)	75.51	75.51	75.51	75.51
		Stain. steel (7.9g/cm^3)	13.37	13.72	13.90	13.94
		Air	11.12	11.77	10.59	10.55
	Upper blanket	U^{238} (18.8g/cm^3)	75.51	75.51	75.51	75.51
		Stain. steel (7.9g/cm^3)	11.06	12.43	12.43	6.84
		Air	13.43	12.06	12.06	17.65

Equivalent diameter – the diameter of the circle whose area equals to the area of assembly's cross-section.

-I2-

Table II

	BFS-1A		BFS-6A		BFS-8		BFS-12	
	Exper.	Calcul.	Exper.	Calcul.	Exper.	Calcul.	Exper.	Calcul.
Critical mass kg U^{235}	76.5	78.2	239.5	248	343.8	323	709.4	682
f_8^{a3}/f_5^{a3}	0.009±0.001	0.010	0.26±0.02	0.27	0.0034±0.0001	0.0042	0.100±0.005	0.123
f_8^{a3}/f_5^{a3}	0.17±0.02	0.17	0.092±0.007	0.085	0.093±0.007	0.099	0.083±0.004	0.065
a_8^{a3}/f_5^{a3}	0.009±0.0006	0.0119	0.75±0.04	0.79	0.0133±0.0007	0.0140	0.57±0.03	0.57
a_8^3/f_5^{a3}	1.38±0.14	1.44	1.15±0.08	0.9	1.28±0.09	1.19	0.85±0.05	0.88
Breeding ratio	1.21±0.15 $\alpha = 0.15$	1.27	1.57±0.11 $\alpha = 0.21$	1.40	1.07±0.08 $\alpha = 0.21$	1.00	1.13±0.07 $\alpha = 0.254$	1.15

f — fission integral; a — capture integral; c — core; b — blanket; 8 — U^{238}; 5 — U^{235}

Table III

			BFS-1A	BFS-6A	BFS-8	BFS-12
$\dfrac{\Delta K}{K}$	$\dfrac{\Delta M_\epsilon}{M}$	(Calcul)	0.52	0.44	0.52	0.45
$\dfrac{\Delta K}{K}$ /	$\dfrac{\Delta M_R}{M}$	(Exper)	0.21	0.15	0.23	0.14
$\dfrac{\Delta K}{K}$ /	$\dfrac{\Delta M_R}{M}$	(Calcul)	0.23	0.14	0.22	0.15

ΔM_ϵ — the variation of critical mass with the uniform variation of partial volume of fissionable isotope.

ΔM_R — the variation of critical mass with the variation of core's radius — $\dfrac{\Delta M}{M} = \dfrac{2\Delta R}{R}$

Table IV

	BFS-1A		BFS-6A		BFS-8		BFS-12	
	Exper.	Calcul.	Exper.	Calcul.	Exper.	Calcul.	Exper.	Calcul.
x_H^2	0.013±0.001	0.01459	0.0050±0.0003	0.00531	0.0024±0.0002	0.002844	0.0017±0.0002	0.001891
$\bar\sigma^8(n_1 f)/\bar\sigma^5(n_1 f)$	0.081±0.005	0.093	0.042±0.002	0.0414	0.036±0.001	0.039	0.0254±0.0003	0.0293
$\bar\sigma^8(n_1\gamma)/\bar\sigma_5(n_1 f)$	0.084±0.007	0.100	0.106±0.006	0.114	0.114±0.006	0.12	0.129±0.006	0.129
$\bar\sigma^9(n_1 f)/\bar\sigma_5(n_1 f)$	–	–	1.16±0.02	1.176	1.27±0.02	1.15	1.03±0.02	1.0148
$\bar\sigma^3(n_1 f)/\bar\sigma_5(n_1 f)$	–	–	1.59±0.02	1.518	1.56±0.02	1.53	1.51±0.02	1.454
$\bar\sigma^2(n_1 f)/\bar\sigma_5(n_1 f)$	–	–	0.0100±0.0015	0.00806	–	–	–	–
$\bar\sigma^7(n_1 f)/\bar\sigma^5(n_1 f)$	–	–	–	–	–	–	0.155±0.012	0.211

Reactivity coefficients for the center of reactor (10^{-3}/kg)

Table V

Material	BFS-1A		BFS-6A		BFS-8		BFS-12	
	Exper.	Calcul.	Exper.	Calcul.	Exper.	Calcul.	Exper.	Calcul.
U^{235}	+14.43±0.8	+12.3	+6.09±0.05	+5.21	+3.46±0.03	+3.26	+2.05±0.03	+2.11
U^{238}	+1.24±0.1	+1.19	−0.267±0.009	−0.261	−0.015±0.011	−0.093	−0.14±0.01	−0.145
Pu^{239}	+29.3±0.7	+22.6	+11.0±0.15	+8.66	+5.96±0.13	+5.63	+8.31±0.13	+3.19
Iron	+0.49±0.05	+0.59	−0.18±0.02	−0.265	−0.10±0.03	+0.02	−0.035±0.023	−0.0445
Stainl.steel	0.21+0.05	+0.50	−0.20±0.02	−0.29	+0.028±0.026	+0.014	−0.04±0.02	−0.053
Aluminium	–	–	−0.37±0.06	−0.262	+0.40±0.08	+0.32	0.008±0.07	−0.0277
Graphite	+10.5±0.30	+8.1	+0.27±0.10	+0.134	+2.6±0.15	+1.54	+0.0302±0.11	+0.175
Nickel	−0.8±0.1	−0.4	−0.39±0.02	−0.402	–	–	−0.049±0.02	−0.0995
B_4C (Natural)	–	–	−9.56±0.34	−7.00	−5.16±0.23	−4.88	−5.8±0.24	−5.42

Composition of uranium oxide prism

Table VI

Element	Uranium	Oxygen	Iron	Hydrogen
Number of nuclei per cm^3 x 10^{-22}	0.902	2.63	0.373	0.014

368

-15-

Parameters of asymptotic spectra in uranium and uranium-containing media

Table VII

Medium Parameter	Metallic uranium		$UC_{0.884}$		$UO_{2.92}Fe_{0.41}H_{0.015}$	
	Exper.	Calcul.	Exper.	Calcul.	Exper.	Calcul.
$\sigma_f(U^{238})/\sigma_f(U^{235})$	1.53±0.06	1.44	1.38±0.06	1.29	1.44±0.06	1.25
$\sigma_f(Pu^{239})/\sigma_f(U^{235})$	0.93±0.04	0.96	0.79±0.03	0.84	0.93±0.04	0.89
$\sigma_f(U^{238})/\sigma_f(U^{235})$	0.0027±0.0003	0.0026	0.0026±0.0002	0.0026	0.0024±0.0003	0.0026
$\sigma_c(U^{238})/\sigma_f(U^{235})$	0.126±0.008	0.129	0.118±0.009	0.096	0.12±0.01	0.10
$\sigma_c(Au^{197})/\sigma_f(U^{235})$	0.26±0.03	0.31	0.70±0.05	0.74	0.58±0.10	0.51
$\sigma_c(Na^{23})/\sigma_f(U^{235})$	–	–	0.0017±0.0001	0.0018	–	–
$\sigma_{np}(S^{32})/\sigma_f(U^{235})$	–	–	0.00049±0.00003	0.00048	–	–
$\mathcal{Z}/N_8$ (barns)	2.30±0.03	2.30	3.30±0.06	3.40	5.50±0.05	5.59

The measurements were made by thick gold indicators and resonance selfshielding of gold cross-sections was to be taken into account.

Parameters of equilibrium spectra in uranium-containing media and thorium

Table VIII

Medium Parameter	Metallic uranium		$UC_{0.884}$		Metallic thorium	
	Exper.	Calcul.	Exper.	Calcul.	Exper.	Calcul.
$\sigma_f(U^{233})/\sigma_f(U^{235})$	1.56±0.05	1.46			1.57±0.06	1.50
$\sigma_f(Pu^{239})/\sigma_f(U^{235})$	1.07±0.04	1.08	0.90±0.04	0.89	1.04±0.05	1.11
$\sigma_f(U^{238})/\sigma_f(U^{235})$	0.0169±0.0007	0.0170	0.0130±0.0008	0.0133	0.0172±0.0009	0.0188
$\sigma_f(Th^{232})/\sigma_f(U^{235})$	–	–	0.0026±0.0002	0.00236	0.0032±0.0002	0.0034
$\sigma_c(U^{238})/\sigma_f(U^{235})$	0.121±0.005	0.122	0.124±0.006	0.118		
$\sigma_c(Th^{232})/\sigma_f(U^{235})$	–	–	–	–	0.135±0.007	0.155
$\sigma_c(Au^{197})/\sigma_f(U^{235})$	0.25±0.01	0.23	0.57±0.05	0.48		
$\sigma_c(Na^{23})/\sigma_f(U^{235})$	–	–	0.0017±0.0001	0.0015		
D	0.173±0.005	0.171	0.15±0.01	0.15	0.029±0.001	0.025

The Additional Reflector Efficiency

Table IX

Blanket material Reflector material	Uranium metallic B	Uranium-carbon composition			Thorium metallic	
		Λ	B	Λ	B	Λ
Water	0.49±0.10	14	0.26±0.06	5.8	0.46±0.10	10.7
Berillium	0.86±0.10	34.6	0.54±0.08	21.9	0.75±0.10	22.1
Carbon	--	--	0.50±0.08	17.9	0.55±0.09	13.5
Iron	0.28±0.09	6.4	0.42±0.07	12.8	0.24±0.07	5.1
Nickel	0.51±0.10	14.9	0.47±0.07	15.6	0.36±0.08	7.9
Copper	0.41±0.09	10.8	0.24±0.06	5.9	0.26±0.07	5.5
Stainless steel 1 x 18H9T	0.40±0.09	10.6	0.33±0.06	9.2	0.30±0.8	6.5

Comparison of experimental and calculated values
of capture and fission cross-sections and $\alpha = \sigma_c/\sigma_f$
for central samples of U^{233}, U^{235} and Pu^{239}

Table X

Isotope	Barns		Barns		Barns	
	Experim.	Calcul.	Experim.	Calcul.	Experim.	Calcul.
U^{233}	0.155±0.015	1.165	2.26±0.10	2.22	0.07±0.01	0.074
U^{235}	0.280±0.020	0.257	1.48±0.06	1.48	0.19±0.02	0.174
Pu^{239}	0.200±0.015	1.168	1.81±0.05	1.81	0.11±0.01	0.093

Experimental value of σ_f received by comparison of the number of fission events in U^{233}, U^{235} and Pu^{239} samples. For the latter the fission cross-section was chosen to be equal to calculated: 1.81 barns.

Comparison of Experimental and Calculated Values
of Capture Cross-sections for Central Samples of
U^{238} and Pu^{240}

Table XI

Isotope	σ_c (barns)	
	Experiment	Calculation
Uranium-238	0.17±0.02	0.164
Plutonium-240	0.24±0.02	0.310

Comparison of Experimental and Calculated Values
of $\alpha = \sigma_c/\sigma_f$ for the Samples of U^{235} and Pu^{239}
Placed at the Distances 16.5 cm and 45.8 cm from
the Core Centre

Table XII

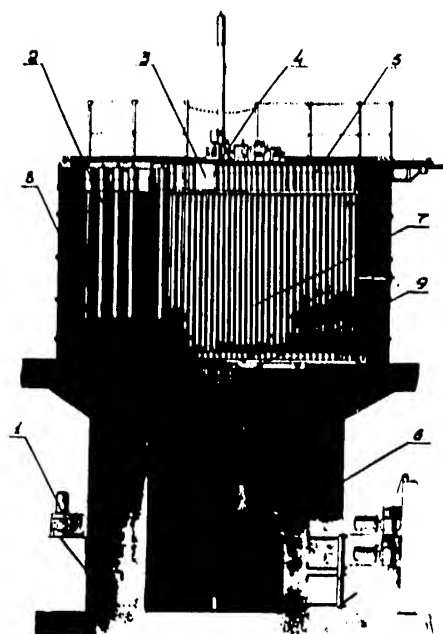| Isotope	r = 16.5 cm		r = 45.8 cm	
	Experim.	Calc.	Experim.	Calc.
Uranium-235	0.33±0.03	0.37	0.55±0.05	0.61
Plutonium-239	0.38±0.04	0.40	0.75±0.08	0.67

-I6-

FIG.I. VERTICAL SECTION OF THE BFS STAND. I - CONTROL ROD ACTU-
ATOR. 2 - EXPERIMENTAL CHANNEL OF THE THERMAL COLUMN. 3 - TRANS-
PORTABLE FACE SHIELDING. 4 - THE ARRANGEMENT FOR DISPLACEMENT OF
DETECTORS. 5 - MEASUREMENT CHANNEL IN THE FACE SHIELDING. 6 - LO-
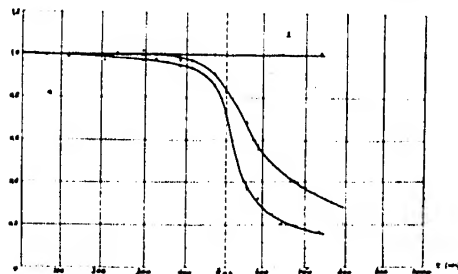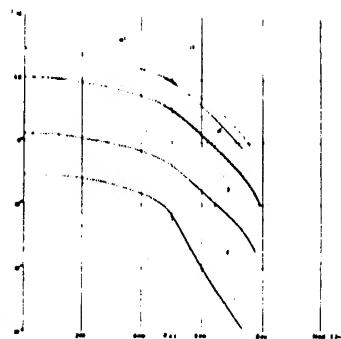WER BOX. 7 - FUEL ROD. 8 - THERMAL COLUMN 9.- CONTROL ROD.

FIG.2. RADIAL DISTRIBUTION OF DIFFERENT REACTION
AT BFS-I2 STAND. Ia - U^{255} (n,f) IN FACE SHIELD-
ING AT 62.2 CM HEIGHT FROM CENTRAL PLANE. Ib-U^{255}
(n;f) AT CENTRAL PLANE OF THE REACTOR. 2 -$U^{235}(n,f)$
3 - $U^{255}(n,f)$. SOLID CURVE IS CALCULATED BY THE
METHOD OF APPROXIMATE SEPARATION OF THE VARIABLES
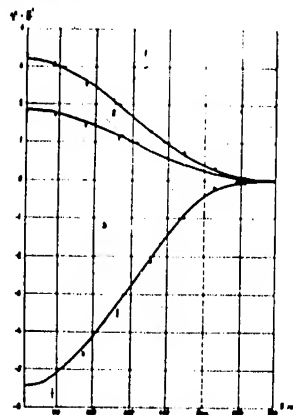DUSHED CURVE PRESENTS THE RESULTS OF TWO-DIMENSI-
ONAL CALCULATION.

FIG.3. RELATIVE CROSS-SECTIONS OF DIFFERENT REACTIONS IN BFS-I2
STAND. I. $\oplus - \dfrac{\sigma_f(Pu^{239})}{\sigma_f(U^{235})}$ 2. $\oplus - \dfrac{\sigma_f(Np^{239})}{\sigma_f(U^{235})}$ 3. $\oplus - \dfrac{\sigma_f(U^{238})}{\sigma_f(U^{235})}$

FIG.4. RADIAL DISTRIBUTION OF THE PERTURBA-
TIONS IN BFS-I2 STAND. I - Pu^{239}. 2 - U^{25}
(90% ENRICHMENT). 3 - B_4C (NATURAL). SOLID
CURVE: IS CALCULATED BY APPROXIMATE SEPARA-
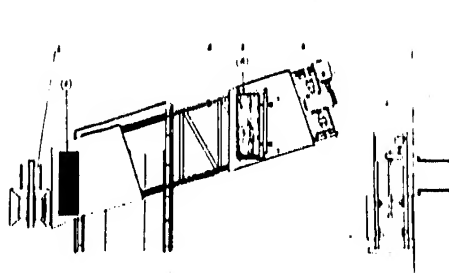TION OF VARIABLES, CIRCLES CORRESPOND TO
EXPERIMENT.

368

-I7-

FIG.5. THE GEOMETRY OF EXPERIMENTAL DEVOTED TO MEASUREMENT OF SPECTRA OF THE NEUTRONS EMERGING FROM NICKEL PRISM BY THE TIME-OF-FLIGHT TECHNIQUE. I - THE CORE OF IBR REACTOR. 2 - THE PRISM INVESTIGATED. 3 - DISTANTLY REMOVABLE PLATFORM. 4 - THE GATE OF EVACUATED NEUTRON FLIGHT PATH. 5 - THE ENTRANCE OPENING OF EVACUATED NEUTRON FLIGHT PATH IOOO METRES LENGTH. 6 - PLATFORM ACTUATOR. A - PRISM'S INVESTIGATION, B - PRISM'S OFF-POSITION.
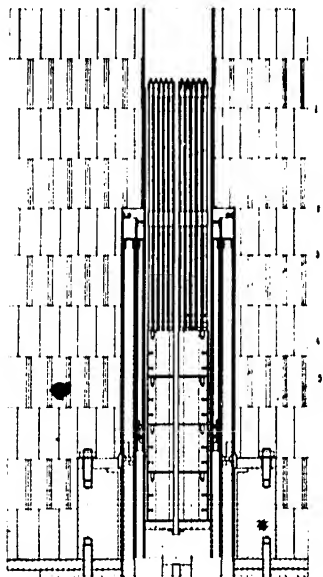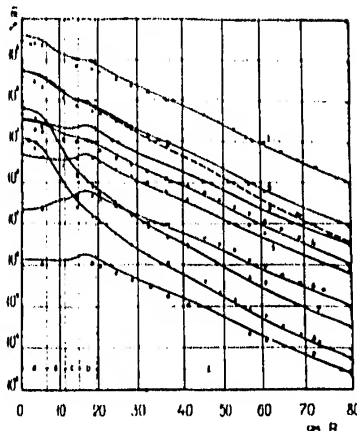

FIG.6. THE DISTRIBUTION OF DIFFERENT REACTIONS IN BR-I REACTOR WITH URANIUM-GRAPHITE BLANKET. POINTS PRESENT EXPERIMENTAL VALUES. SOLID LINE REPRESENTS THE CALCULATED RESULTS WHEN TRANSPORT P3 - APPROXIMATION AND SPHERICAL GEOMETRY HAVE BEEN USED. ALL THE DATA ARE RENORMALIZED TO THE SAME REACTOR POWER LEVEL. A - THE CORE, B - URANIUM CONTROL RODS, C - URANIUM RING, D - GRAPHITE GEHAGON, E - URANIUM GRAPHITE BLANKET.
I - $U^{235}(n,f)$ x IO. 2 - $Pu239(n,f)$; 2a - $Pu^{239}(n,f)$. 3 - $U^{238}(n,\gamma)$. 4 - $U^{238}(n,f)$. 5 - $Au^{197}(n,\gamma)$xIO . 6 - $Mn^{55}(n,\gamma)$xIO . 7- $U^{238}(n,f)$. 8 - $Th^{232}(n,f)$. 9 - $Na^{23}(n,f)$. THE EFFECTS OF RESONANCE CROSS-SECTION SELFSHIELDING OF THE MEDIUM WERE NOT CONSIDERED.

FIG.8. THE CONSTRUCTION OF CENTRAL REGION OF THE BR-I REACTOR WITH THORIUM BLANKET. I - THE TAGS FORMING UPPER PLANE BLANKET. 2 - PLUTONIUM RODS. 3 - CONTROL RODS. 4 - LOWER PLANE THORIUM BLANKET. 5 - THORIUM SLAGS.
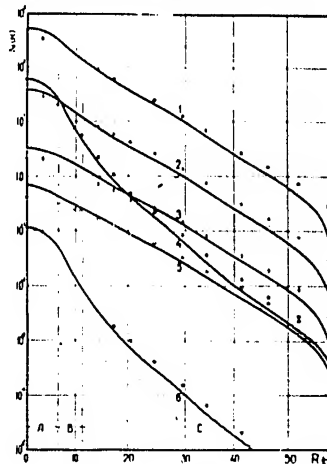

FIG.7. THE DISTRIBUTION OF DIFFERENT REACTIONS IN BR-I REACTOR WITH URANIUM METAL BLANKET. POINTS SHOW THE EXPERIMENTAL RESULTS. CALCULATION DATA AT TRANSPORT P3-APPROXIMATION IN SPHERICAL GEOMETRY ARE PRESENTED BY SOLID CURVE. ALL THE DATA ARE RENORMALIZED TO THE SAME REACTOR POWER LEVEL. A - THE CORE, B - URANIUM CONTROL RODS, C - URANIUM BLANKET. I - $Pu^{239}(n,f)$. 2 - $U^{235}(n,f)$. 3 - $U^{238}(n,\gamma)$. 4 - $U^{238}(n,f)$. 5 - $Au^{197}(n,\gamma)$. 6 - $Th^{232}(n,f)$.
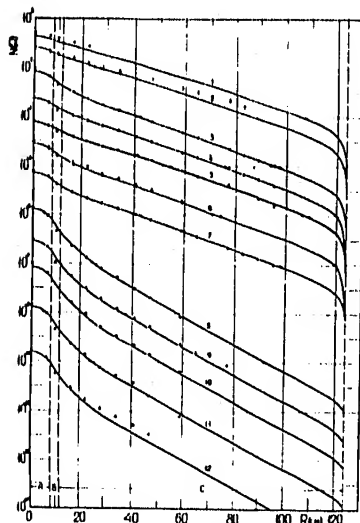
368

-I8-

FIG.9. THE DISTRIBUTION OF DIFFERENT REACTIONS IN THE BR-I REACTOR WITH THORIUM BLANKET. POINTS CORRESPOND TO EXPERIMENT. THE DATA CALCULATED IN TRANSPORT P_3-APPROXIMATION IN SPHERICAL GEOMETRY ARE SHOWN BY SOLID CURVES. ALL THE DATA ARE RENORMALIZED TO THE SAME REACTOR POWER LEVEL. A - THE CORE, B - THORIUM CONTROL RODS, C - THORIUM BLANKET. I - $Mn^{55}(n,\gamma) \times 10^5$. 2 - $Au^{197}(n,\gamma) \times 10^2$. 3 - $Pu^{239}(n,f)$. 4 - $Th^{232}(n,\gamma)$. 5 - $Cu^{63}(n,\gamma)$. 6 - $U^{235}(n,f) \times 10^{-3}$. 7 - $U^{235}(n,f) \times 10^{-4}$. 8 - $Th^{232}(n,f)$. 9 - $U^{238}(n,f) \times 10^{-7}$. 10 - $P^{31}(n,p) \times 10^{-7}$. II - $S^{32}(n,p) \times 10^{-9}$. I2 - $Si^{28}(n,p) \times 10^{-10}$.

FIG.10. THE DENSITY DISTRIBUTION OF DIFFERENT REACTION IN THE BR-I REACTOR WITH NICKEL BLANKET. POINTS SHOW THE EXPERIMENTAL DATA. THE RESULTS OF CALCULATION CARRIED OUT IN TRANSPORT P_3-APPROXIMATION IN SPHERICAL GEOMETRY BY USING THE CONSTANTS FROM 4 WITHOUT THE CONSIDERATION OF SELFSHIELDING EFFECTS ARE SHOWN BY DASHED-POINTED CURVE. THE SAME RESULTS AFTER TAKING INTO ACCOUNT THE RESONANCE SELFSHIELDING EFFECTS ARE REPRESENTED BY DASHED CURVE. SOLID CURVE CORRESPONDS TO CORRECT VALUES OF CONSTANTS (SEE THE TEXT). ALL THE DATA RENORMALIZED TO THE SAME REACTOR POWER LEVEL. A - THE CORE, B - CONTROL RODS, C - NICKEL HEXAGON, D - BLANKET CONSISTING OF NICKEL SLUGS. I - $Pu^{239}(n,f)$. 2 - $Au^{197}(n,\gamma)$. 3 - $Mn^{55}(n,\gamma)$. 4 - $Th^{232}(n,f)$. 5 - $Cu^{63}(n,\gamma)$. 6 - $Na^{23}(n,\gamma)$.
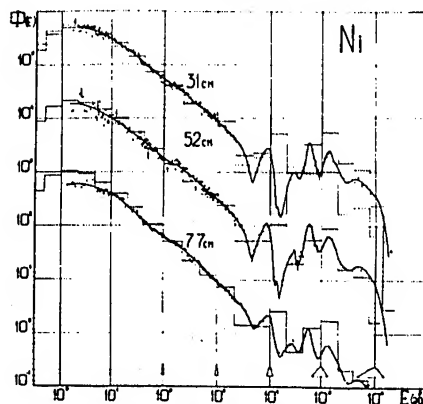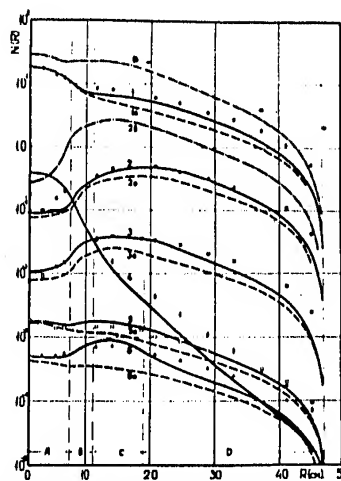

FIG.II. THE SPECTRUM OF NEUTRONS EMERGING FROM THE NICKEL PRISM OF VARIOUS THICKNESS. THE CALCULATION RESULTS CARRIED OUT IN TRANSPORT S_8-APPROXIMATION IN PLANE GEOMETRY SHOWN BY HISTOGRAMS. SOLID HISTOGRAM CORRESPONDS TO CALCULATION TAKING INTO ACCOUNT RESONANCE SELFSHIELDING OF NICKEL CROSS-SECTION, DASHED - WITHOUT CONSIDERATION OF THIS EFFECT.
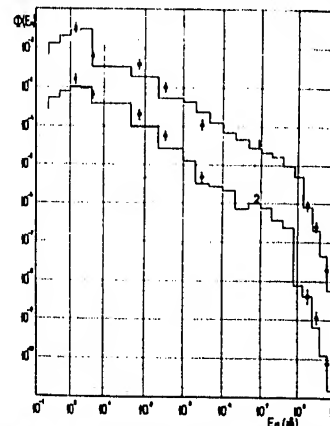

FIG.12. NEUTRON SPECTRA IN THE NICKEL BLANKET OF BR-I REACTOR AT 14.4 cm (CURVE I) AND 29 cm (CURVE 2) FROM CENTRE. POINTS SHOW THE EXPERIMENTAL DATA FOR THRESHOLD-DETECTORS $Th^{232}(n,f)$, $P^{31}(n,p)$ AND $Si^{28}(n,p)$ AND FOR RESONANCE INDICATORS $In^{115}(1.44ev)$ $Au^{197}(4.9ev)$, $La^{139}(73.5ev)$, $Mn^{55}(337ev)$ AND $Na^{23}(2.9$ Kev). THE HISTOGRAMS DEMONSTRATE THE RESULTS OF CALCULATIONS CARRIED OUT IN TRANSPORT P_3-APPROXIMATION IN SPHERICAL GEOMETRY. THE CORRECTED SELFSHIELDING FACTORS ARE USED FOR THE CROSS-SECTIONS. ALL THE DATA RENORMALIZED TO THE SAME REACTOR POWER LEVEL.
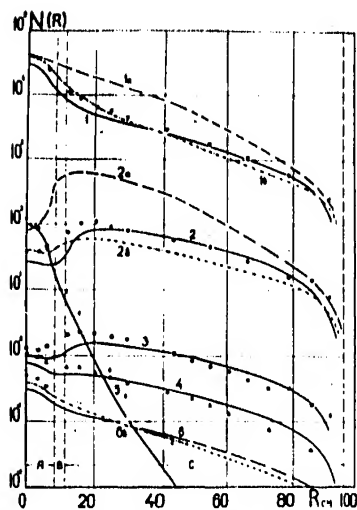
368

-19-

FIG.13. THE DISTRIBUTION OF DIFFERENT REACTIONS IN
BR-I REACTOR WITH IRON BLANKET. POINTS SHOW THE EXPE-
RIMENTAL DATA. THE RESULTS OF CALCULATED CARRIED OUT
IN TRANSPORT P_3-APPROXIMATION IN SPHERICAL GEOMETRY
WITH NO CONSIDERATION OF SELFSHIELDING EFFECTS ARE
SHOWN BY DASHED CURVE. THE SAME CALCULATIONS TAKING
INTO ACCOUNT THE EFFECTS OF CROSS-SECTION RESONANCE
SELFINDICATION ARE SHOWN BY SOLID CURVE. THE RESULTS
OF TWO DIMENSIONAL CALCULATION IN P_3-APPROXIMATION ARE
SHOWN BY DASHED POINTED CURVE. A - THE CORE, B - IRON
CONTROL RODS, C - IRON BLANKET. I - $Pu^{239}(n,f)$. 2 -
$Au^{197}(n,)$. 3 - $Mn^{55}(n,)$. 4 - $Na^{23}(n,)$. 5 - Th^{232}
$(n,f) \times 10$. 6 - $Cu^{63}(n,) \times 10^{-2}$.

FIG.14. THE NEUTRON SPECTRA EMERGING FROM THE IRON PRISM
OF VARIOUS THICKNESS. THE HISTOGRAMS SHOW THE RESULTS OF
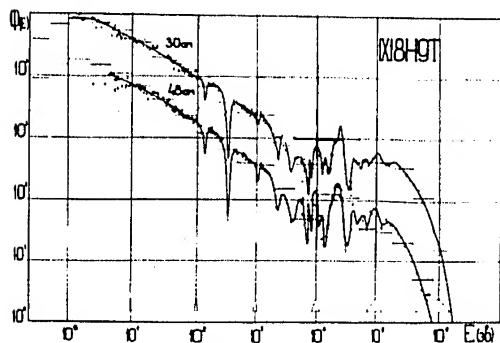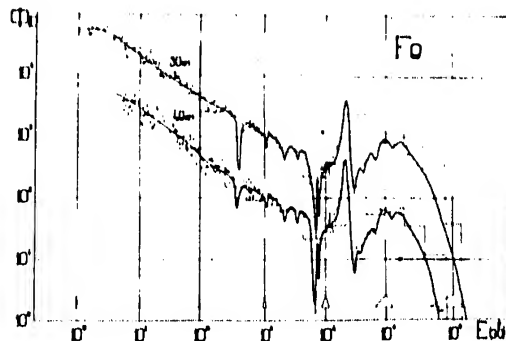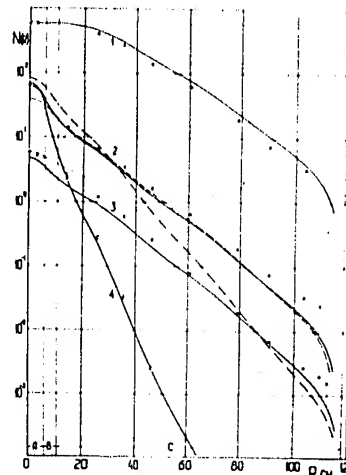CALCULATIONS CARRIED OUT IN TRANSPORT S_8-APPROXIMATION
IN PLANE GEOMETRY.

FIG.15. THE NEUTRON SPECTRA EMERGING FROM THE STAINLESS
STEEL PRISM. THE HISTOGRAMS SHOW THE RESULTS OF CALCULA-
TIONS CARRIED OUT IN TRANSPORT S_8-APPROXIMATION IN PLA-
NE GEOMETRY.

FIG.16. DENSITY DISTRIBUTION OF SOME REACTIONS IN
BR-I REACTOR WITH COPPER BLANKET. POINTS CORRES-
POND TO EXPERIMENTAL VALUES. THE RESULTS OF CAL-
CULATIONS IN TRANSPORT P_3-APPROXIMATION IN SPHE-
RICAL GEOMETRY (SOLID CURVE) AND TWO-DIMENSIONAL
CALCULATIONS IN P_1-APPROXIMATION (DASHED CURVE)
ARE PRESENTED. ALSO THE CALCULATION RESULTS FOR
$Cu^{63}(n,)$ REACTION WITH NO CONSIDERATION OF SELF-
SHIELDING EFFECT ARE SHOWN BY POINTED CURVE. DA-
SHED-POINTED CURVES CALCULATED WITHOUT TAKING IN-
TO ACCOUNT THE CROSS-SECTION SELFSHIELDING EFFEC-
TS. A - THE CORE, B - GERMAN SILVER CONTROL RODS,
C - COPPER BLANKET.
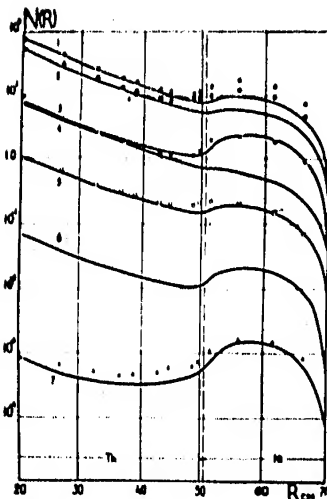I - $Au^{197}(n,)$. 2 - $Pu^{239}(n,f)$. $Cu^{63}(n,)$. 4 -
$U^{238}(n,f)$.

368

-20-

FIG.17. THE DENSITY DISTRIBUTION OF SOME REACTIONS AT THORIUM-NICKEL BOUNDARY. POINTS SHOW THE EXPERIMENTAL VALUES. THE RESULTS OF TRANSPORT P₃-APPROXIMATION, IN SPHERICAL GEOMETRY ARE PRESENTED BY SOLID CURVES. 1-U235(n,f). 2 - U235(n,f). 3 - Th232(n,). 4- Th232(n,). 5 - Au197(n,). 6 - U235(n,). 7 - THE CONTRIBUTION OF GOLD RESONANCE AT 4.9 ev INTO THE SAMPLE ACTIVATION. THE DISCREPANCY OF U235 (n,f) AND U235(n,f) DISTRIBUTIONS COULD BE EXPLAINED BY THE UNCERTAINTIES IN NICKEL CONSTANTS USED FOR THE CALCULATION.
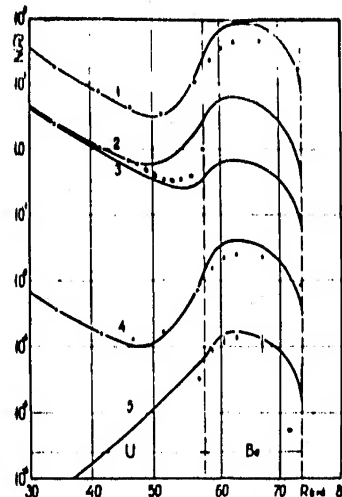

FIG.18. THE DENSITY DISTRIBUTION OF VARIOUS REACTIONS AT URANIUM-BERYLLIUM BOUNDARY. POINTS SHOW THE EXPERIMENTAL VALUES . THE RESULTS OF CALCULATIONS CARRIED OUT IN TRANSPORT P₃-APPROXIMATION IN SPHERICAL GEOMETRY ARE SHOWN BY SOLID CURVES. 1.U235(n,f). 2.U238(n,). 3.U238(n,). 4.Au197 5. THE CONTRIBUTION OF GOLD RESONANCE AT 4.9 ev INTO SAMPLE ACTIVATION. THE DISAGREEMENT IN THE CASE OF U235(n,f) DISTRIBUTION CAUSED BY IMPURITIES OF BERYLLIUM USED.
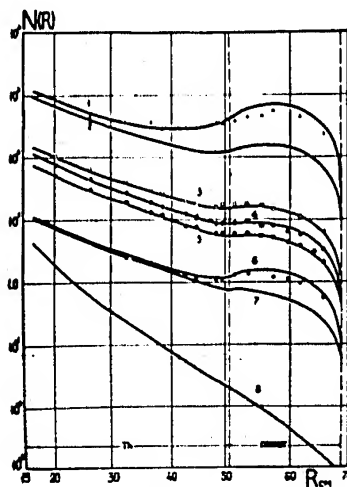
FIG.19. THE DENSITY DISTRIBUTION OF DIFFERENT REACTIONS AT STAINLESS STEEL - THORIUM BOUNDARY. POINTS SHOW THE EXPERIMENTAL DATA. THE RESULTS OF CALCULATION IN TRANSPORT P₃-APPROXIMATION IN SPHERICAL GEOMETRY ARE PRESENTED BY SOLID CURVES.
I. Au197(n,). 2/

I. Au197(n,)x10¹². 2. U235(n,)x10². 3. Cu63(n,f) x10⁵. 4. U235(n,f). 5. U235(n,f). 6. Th232(n,). 7. Th232(n,). 8. Th232(n,f).

FIG.20. NEUTRON SPECTRA IN BR-5 REACTOR AT VARIOUS DISTANCES FROM THE CENTRE. SOLID HISTOGRAM SHOWS THE SPECTRUM OF NEUTRON FLUX; DASHED HISTOGRAM PRESENTS THE DISTRIBUTIONS OF CAPTURE EVENTS IN Pu239.

368

-21-

FIGURE CAPTIONS

Fig.1. Vertical Section of the BFS Stand.

    1. Control rod actuator.

    2. Experimental channel of the thermal column.

    3. Transportable face shielding.

    4. The arrangement for displacement of detectors.

    5. Measurement channel in the face shielding.

    6. Lower box.   8. Thermal column.

    7. Fuel rod.   9. Control rod.

Fig.2. Radial distribution of different reaction at BFS-12 stand.

    1a. U^{235} (n, f) in face shielding at 82.2cm height from central plane.

    1b. U^{235} (n, f) at central plane of the reactor.

    2. U^{238} (n, f)   3. U^{238} (n, γ)

    Solid curve is calculated by the method of approximate separation of the variables.

    Dashed curve presents the results of two-dimensional calculation.

Fig.3. Relative cross-sections of different reactions in BFS-12 stand.

$$1. \circ - \frac{\sigma_f\,(Pu^{239})}{\sigma_f\,(U^{235})} \qquad 2. \bullet - \frac{\sigma_f\,(Np^{237})}{\sigma_f\,(U^{235})} \qquad 3. \; \bullet - \frac{\sigma_f\,(U^{238})}{\sigma_f\,(U^{235})}$$

Fig.4. Radial distribution of the perturbations in BFS-12 stand.

    1. Pu^{239}, 2. U^{235} (90% enrichment), 3. B_4C (natural). Solid curve is calculated by approximate separation of variables, circles correspond to experiment.

Fig. 5. The geometry of experiment devoted to measurement of spectra of the neutrons emerging from nickel prism by the time-of-flight technique.

    1. The core of IBR reactor. 2. The prism investigated. 3. Distantly removable platform. 4. The gate of evacuated neutron flight path. 5. The entrance opening of evacuated neutron flight path 1000 metres long. 6. Platform actuator. A — prism's in-position, B — prism's off-position.

Fig.6. The distribution of different reactions in BR-1 reactor with uranium-graphite blanket. Points present experimental values. Solid line represents the calculated results when transport P_3-approximation and spherical geometry have been used. All the data are renormalized to the same reactor power level.

    A — the core, B — uranium control rods, C — uranium ring, D — graphite hexagon, E — uranium graphite blanket.

    1. U^{235} (n, f) x 10; 2. Pu^{239} (n, f); 2a. Pu^{239} (n, f); 3. U^{238} (n, γ); 4. U^{238} (n, γ); 5. Au^{197} (n, γ) x 10^{-1}; 6. Mn^{55} (n, γ) x 10^{-1}; 7. U^{238} (n, f); 8. Th^{232} (n, f); 9. Na^{23}(n, γ).

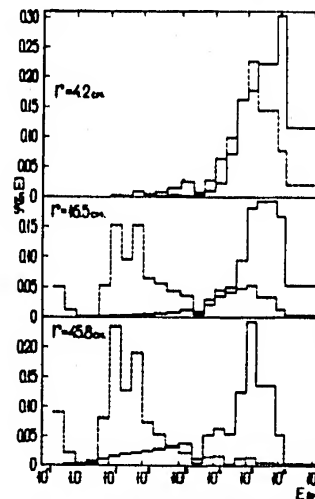The effects of resonance cross-section selfshielding of the medium were not considered.

Fig.7. The distribution of different reactions in BR-1 reactor with uranium metal blanket. Points show the experimental results. Calculation data at transport P_3-approximation in spherical geometry are presented by solid curve. All the data are renormalized to the same reactor power level.

    A — the core, B — uranium control rods, C — uranium blanket.

    1. Pu^{239} (n, f); 2. U^{235} (n, f); 3. U^{238} (n, γ); 4. U^{238} (n, f); 5. Au^{197} (n, γ); 6. Th^{232}(n,f).

Fig.8. The construction of central region of the BR-1 reactor with thorium blanket.

    1. The tags forming upper plane blanket. 2. Plutonium rods. 3. Control rods. 4. Lower plane thorium blanket. 5. Thorium slugs.

368   — 22 —

Fig.9. The distribution of different reactions in the BR-1 reactor with thorium blanket. Points correspond to experiment. The data calculated in transport P_3-approximation in spherical geometry are shown by solid curves. All the data are renormalized to the same reactor power level.

A — the core, B — thorium control rods, C — thorium blanket.

1. Mn^{55} (n, γ) x 10^5; 2. Au^{197}(n, γ) x 10^2; 3. Pu^{239} (n, f); 4. Th^{232} (n, γ); 5. Cu^{63}(n, γ); 6. U^{233} (n, f) x 10^{-3}; 7. U^{235} (n, f) x 10^{-4}; 8. Th^{232} (n, f); 9. U^{238} (n, f) x 10^{-7}; 10. P^{31} (n, p) x 10^{-7}; 11. S^{32} (n,p) x 10^{-9}; 12. Si^{28} (n, p) x 10^{-10}.

Fig.10. The density distribution of different reactions in the BR-1 reactor with nickel blanket. Points show the experimental data. The results of calculation carried out in transport P_3-approximation in spherical geometry by using the constants from [4] without the consideration of selfshielding effects are shown by dashed-pointed curve. The same results after taking into account the resonance selfshielding effects are represented by dashed curve. Solid curve corresponds to corrected values of constants (see the text). All the data renormalized to the same reactor power level.

A — the core, B — control rods, C — nickel hexagon, D — blanket consisting of nickel slugs.

1. Pu^{239} (n, f); 2. Au^{197} (n, γ); 3. Mn^{55} (n, γ); 4. Th^{232} (n, f); 5. Cu^{63} (n, γ); 6. Na^{23} (n, γ).

Fig.11. The spectrum of neutrons emerging from the nickel prism of various thickness. The calculation results carried out in transport S_8-approximation in plane geometry shown by histograms. Solid histogram corresponds to calculation taking into account resonance selfshielding of nickel cross-section, dashed — without consideration of this effect.

Fig.12. Neutron spectra in the nickel blanket of BR-1 reactor at 14.4 cm (curve 1) and 29 cm (curve 2) from centre. Points show the experimental data for threshold-detectors Th^{232} (n, f), P^{31} (n, p) and Si^{28} (n, p) and for resonance indicators In^{115} (1.4ev), Au^{197} (4,9ev), La^{139} (73.5ev), Mn^{55} (337ev) and Na^{23} (2.9kev). The histograms demonstrate the results of calculations carried out in transport P_3-approximation in spherical geometry. The corrected selfshielding factors are used for the cross-sections. All the data renormalized to the same reactor power level.

Fig.13. The distribution of different reactions in BR-1 reactor with iron blanket. Points show the experimental data. The results of calculations carried out in transport P_3-approximation in spherical geometry with no consideration of selfshielding effects are shown by dashed curve. The same calculations taking into account the effects of cross-section resonance selfindication are shown by solid curve. The results of two dimensional calculations in P_3-approximation are shown by dashed pointed curve.

A — the core, B — iron control rods, C — iron blanket.

1. Pu^{239} (n, f); 2. Au^{197} (n, γ); 3. Mn^{55} (n, γ); 4. Na^{23} (n, γ); 5. Th^{232} (n, f) x 10; 6. Cu^{63} (n, γ) x 10^{-2}.

Fig.14. The neutron spectra emerging from the iron prism of various thickness. The histograms show the results of calculations carried out in transport S_8-approximation in plane geometry.

Fig.15. The neutron spectra emerging from the stainless steel prism. The histograms show the results of calculations carried out in transport S_8-approximation in plane geometry.

Fig.16. Density distribution of some reactions in BR-1 reactor with copper blanket. Points correspond to experimental values. The results of calculations in transport P_3-approxima-

368

tion in spherical geometry (solid curve) and two-dimensional calculations in P_1'-approximation (dashed curve) are presented. Also the calculation results for Cu^{63} (n, γ) reaction with no consideration of selfshielding effect are shown by pointed curve. Dashed-pointed curves calculated without taking into account the cross-section selfshielding effects.

A — the core, B — German silver control rods, C — copper blanket.

1. Au^{197} (n, γ); 2. Pu^{239} (n, f); 3. Cu^{63} (n, γ); 4. U^{238} (n, f).

Fig.17. The density distribution of some reactions at thorium-nickel boundary. Points show the experimental values. The results of transport P_3-approximation in spherical geometry are presented by solid curves.

1. U^{233} (n, f); 2. U^{235} (n, f); 3. Th^{232} (n, γ); 4. $Th^{232}(n, \gamma)$; 5. Au^{197} (n, γ); 6. U^{233} (n, γ); 7. The contribution of gold resonance at 4.9ev into the sample activation. The descrepancy of U^{233} (n, f) and U^{235} (n, f) distributions could be explained by the uncertainties in nickel constants used for the calculations.

selfshielding effects are not considered;
selfshielding effects are taken into account.

Fig.18. The density distribution of various reactions at uranium-berillium boundary. Points show the experimental values. The results of calculations carried out in transport P_3-approximation in spherical geometry are shown by solid curves.

1. U^{235} (n, f); 2. U^{238} (n, γ); 3. U^{238} (n, γ); 4. Au^{197} (n, γ); 5. The contribution of gold resonance at 4.9ev into sample activation. The disagreement in the case of U^{235} (n, f) distribution caused by impurities of berillium used.

The effects of cross-section selfshielding are not considered.
Selfshielding effects are taken into account.

Fig.19. The density distribution of different reactions at stainless steel — thorium boundary. Points show the experimental data. The results of calculation in transport P_3-approximation in spherical geometry are presented by solid curves.

1. Au^{197} (n, γ) x 10^{12}, 2. U^{233} (n, γ) x 10^2, 3. Cu^{63} (n, f) x 10^5, 4. U^{233} (n, f), 5. U^{235} (n, f), 6. Th^{232} (n, γ), 7. Th^{232} (n, γ), 8. Th^{232} (n, f).

The effects of cross-section selfshielding are not considered.
Selfshielding effects are taken into account.

Fig.20. Neutron spectra in BR-5 reactor at various distances from the centre. Solid histogram shows the spectrum of neutron flux; dashed histogram presents the distribution of capture events in Pu^{239}.

368

— 24 —